Infrared Thermography of the Chip-Tool Interface through Transparent Cutting Tools

Thejas Menon and Vis Madhavan*
Department of Industrial & Manufacturing Eng.
Wichita State University
Wichita, Kansas, USA

*Intelligent Systems Division
National Institute of Standards and Technology
Gaithersburg, Maryland, USA

ABSTRACT
In-situ measurement of the chip-tool interface temperature distribution has been carried out while machining titanium alloy Ti-6Al-4V with transparent cutting tools. A low-noise camera sensitive to visible and near infrared (IR) radiation has been used to record the radiation emitted by the interface, and relatively long exposure times are used to obtain the time averaged temperature distribution. The image intensity is converted into temperature with uncertainty less than 10 °C. Emissivity values found in the literature are compensated for emission into the tool. The temperature along the rake face increases with distance from the cutting edge along the chip flow direction, reaching a maximum near the middle of the contact area. For a cutting speed of 1m/s, the time averaged temperature distribution shows a peak temperature of 906 °C. The high accuracy of the measured time averaged temperature distribution makes this a valuable reference data set for validating finite element simulations.

KEYWORDS
Metal cutting, Tool temperature, Infrared thermography, Blackbody calibration, Ti-6Al-4V

INTRODUCTION

The efficiency and productivity of machining is a key component of manufacturing competitiveness. Digital manufacturing, via accurate simulations, is an increasingly significant component of developed nations' plans to sustain and enhance the competitiveness of their manufacturing industries. Accurate knowledge of key inputs is a prerequisite for machining models to be valid. To date, most machining models are validated with not much more than the measured cutting forces and chip thickness. Accurate temperature measurements are of great importance for validating the practical utility of simulations. It is hard to accurately measure the temperature distribution of the cutting tool, especially the peak temperature which is known to occur along the normally inaccessible chip-tool interface.

Infrared (IR) thermography can be used to measure the temperature distribution over a surface without perturbing it. However, it requires optical access to the surface of interest. Optical access to the normally inaccessible chip-tool interface can be gained by making the tool out of a transparent material. The present study is the first successful effort in which Ti-6Al-4V has been cut with transparent tools and the distribution of temperature at the chip-tool interface has been measured.

BACKGROUND

In metal cutting, it is well known that the contact stress along the chip-tool interface is high enough that the front surface of the chip conforms to the tool rake face until it curls out of contact. This is commonly referred to as the sticking friction regime [1]. However, according to direct observations through transparent cutting tools [2,3], as well as slip-line field models [4,5], the work material slides over the tool rake face in what is referred to as a retarded flow zone. The friction leads to rapid heating of the material, over and above the temperature rise in the primary shear zone. The resulting high temperatures are the leading cause

of tool wear.

The commonly used intrinsic thermocouple technique provides the average interface temperature [6]. The extrinsic thermocouple technique provides the temperature where the thermocouple junction is located. Usui et al. [7] used the extrinsic tool work thermocouple technique to map the temperature distribution under one cutting condition through a series of experiments. Such a study is very expensive to carry out on a routine basis. Metallographic techniques [8] and metallography with specially added inclusions [9] can yield an estimate of the temperature distribution along interior sections of the cutting tool.

Infrared thermography has been used to study the temperature distribution over the cutting tool [10,11], the workpiece [12], the chip side face [13,14], and the free surface of the chip (the back surface) [15]. Davies et al. [16] imaged the side faces of the tool and the workpiece, and obtained the one dimensional (1D) temperature distribution along the intersection of the tool rake face and the side planes of the workpiece and tool. Typically, it is found that uncertainty in these measurements is dominated by the uncertainty in emissivity and correct estimates for uncertainty are of the order of 50 °C for a 15 % uncertainty in the emissivity, over a baseline value of 0.14 [16]. Additionally, material near the side faces of the workpiece deforms in plane stress, and the temperatures along the side face are significantly lower than the temperatures along inner planes along which material deforms in plane strain [17].

Muller-Hummel and Lahres [18-20] and Narayanan et al. [21] have attempted to measure the two dimensional (2D) distribution of temperature over the chip-tool interface, by providing optical access to the chip tool interface and carrying out infrared thermography. Muller-Hummel and Lahres used a 0.5 mm thick diamond window located about 100 µm from the cutting edge, along the rake face. The perturbation of the temperature field by the hole beneath the diamond window and by the outstanding thermal conductivity of diamond is a cause for concern. An infrared camera was used to measure the intensity of radiation emitted by different points on the chip surface, in the 8 µm to 12 µm wavelength range. Calibration involved use of a blackbody (BB) to calibrate the optical system, and emissivity measurement of the chip by heating it in a nitrogen atmosphere. Temperatures significantly greater than the melting point of the work material are reported, and the uncertainty in the measurements is not quantified.

Narayanan et al. [21] used cutting tools made of sapphire, which is transparent in the near and mid-IR wavelengths. They imaged the radiation emitted by the chip along the chip-tool interface, and estimated the temperature using the dual wavelength ratio technique to handle the unknown emissivity of the chip face. The results of the ratio technique showed that the regions where chip material got stuck to the rake face, forming deposits on the rake face, had higher temperatures. Significant challenges are encountered during calibration of the infrared images for conversion into temperature. One source of uncertainty is that, if the two bands of radiation chosen are widely spaced, in order to cause the ratio to change faster with temperature, it cannot be assumed that the emissivity remains the same in the two wavelengths.

Hijazi et al. [14] found that non-greybody behavior of low emissivity surfaces can lead to significant systematic error in dual-wavelength IR thermometry and developed procedures to measure the non-grey body compensation factor (NGCF). It was also found that any error in NGCF would be amplified in the temperature measurements, whereas, the error in emissivity in single wavelength thermography gets reduced by the exponent relating the temperature to intensity. For these reasons it was concluded that single wavelength thermography can result in more accurate measurements, especially if temperatures are high enough that near IR thermography can be carried out for which the exponent relating the intensity to temperature is very high.

EXPERIMENTAL PROCEDURE

Orthogonal cutting of tubes is carried out using the experimental arrangement shown in **Figure 1**. The cutting tool is held stationary while a rotating tube of outer diameter 25.4 mm (1 in) and 1.2 mm wall thickness is fed into the tool. The tubes are prepared from solid rods of solution-treated and annealed Ti-6Al-4V. In a typical cutting experiment, the tube is fed into the tool at constant feed rate for four full revolutions, is held in place for one revolution for a clean-up cut at zero feed, and withdrawn. During the first revolution the depth of cut increases linearly so that the orthogonal cutting depth-of-cut becomes equal to the feed per revolution. The depth of cut remains constant at the value of the feed for three revolutions. The feed is then stopped, which causes the depth of cut to ramp down to zero over one revolution.

A cube with 90° wedge angle for each of the edges,

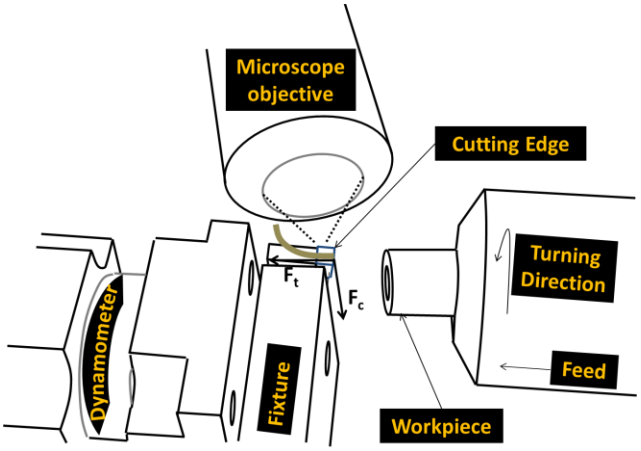

Figure 1 Schematic sketch of the experimental setup

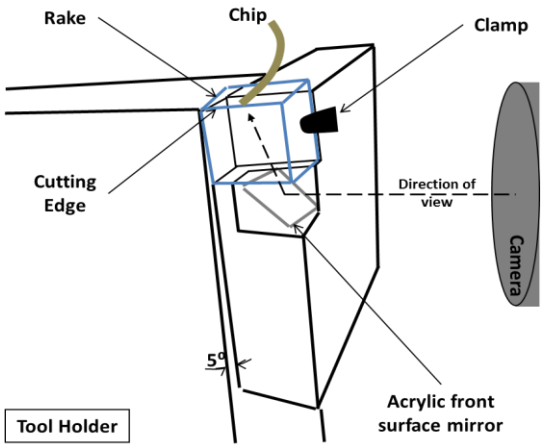

Figure 2 Fixture for the transparent tools, the mirror, and the viewing direction of the camera for imaging the chip-tool interface in-situ while cutting is going on

made of YAG (Yittrium Aluminum Garnet), is used as the cutting tool. The cutting edge of the tool has a 45° chamfer measuring ~30 µm on the rake and flank faces. A fixture holds the tool at –5° rake angle and 5° clearance angle. The fixture allows tools to be changed without disturbing the optical arrangement. It is mounted on a triaxial dynamometer that measures the cutting and thrust forces.

Radiation emitted by the hot chip surface while it is sliding over the rake face of transparent cutting tools is imaged through the tool. The tool holder has a small pocket (as shown in **Figure 2**) which accommodates a front-surface mirror that reflects the radiation emitted by the surface of the chip in contact with the tool towards the viewing direction. YAG has higher hardness and strength than sapphire at high temperatures [22] and is completely transparent at wavelengths from 0.4 µm to 4 µm, with negligible absorption. The simplified cubic geometry simplifies the optical arrangement and causes the effect of internal reflections to be negligible.

The radiant intensity data is imaged during the middle of the three revolutions at steady state depth-of-cut (i.e., over the second revolution at steady state). The exposure times were 80 ms and 40 ms for cutting speeds of 1 m/s and 2 m/s, respectively. The radiation is imaged by a cooled low noise camera [23] that is mounted on a stereomicroscope [24]. A 1x objective, a 1.5x coupler, and 8x optical zoom lead to a magnification of 12x on the image sensor. Each 6.45 µm square pixel of the sensor images a 0.56 µm square region of the tool surface and the total field of view is 770 µm × 570 µm.

The lab is darkened and the in-situ images are recorded. **Figure 3** shows an actual in-situ image recorded by the camera, in which the lower half of the contact area between the tool and the chip is imaged. In **Figure 3**, it can be seen that both a direct image of the rake face, as well as a reflected image, are formed with mirror symmetry about the

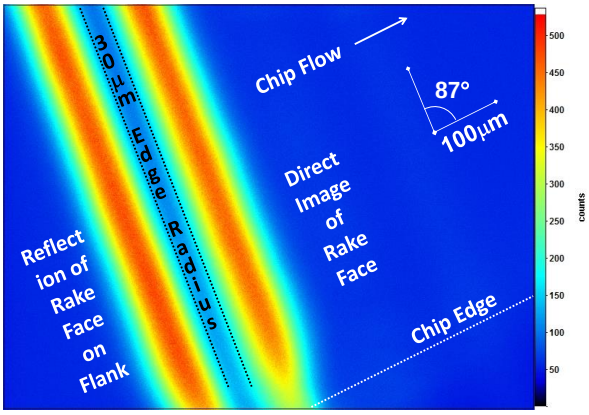

Figure 3 In-situ image of the chip-tool interface at 1 m/s speed and 50 µm feed for a 30 µm edge radius tool

cutting edge, with the chip flowing away from the cutting edge towards the end of chip-tool contact. The direct and reflected images are nearly exact mirror images of one another. Background images at room temperature, taken immediately before cutting, are subtracted pixel-by-pixel from this image of the radiation emitted by the chip. The intensity image is converted to a temperature map using the calibration described next.

CALIBRATION

In the calibration process a miniature blackbody, set at different temperatures between 700 °C and 1000 °C, was imaged through the tool. The calibration process included the steps shown in the flowchart in **Figure 4**, to relate the intensity image of the front surface of the chip to its temperature. In the first step, the radiation emitted by a miniature blackbody source (Electro-Optical Industries, Model 19708-S1) placed in front of the rake face was imaged through the transparent tool. The blackbody was oriented along the viewing direction and brought as close as possible to the tool rake face, until its front face touched one corner of the cutting edge.

The blackbody (BB) was sequentially set to seven equally spaced temperatures between 700 °C to 1000 °C in 50 °C increments, while heating up and while cooling down. At each temperature setting, a settling time of 20 min was allowed before taking three images each at 40 ms and 80 ms exposure times. These were averaged pixel-by-pixel, the background was subtracted, and the average intensity within a 400 µm square box of nominally uniform intensity was obtained. Using shims to create apertures of two different sizes on the rake face of the tool, it was also observed that the counts in the regions covered by the sheet for both aperture sizes showed only a small increase for the larger aperture, indicating that scattering of light within the crystal does not affect the counts significantly.

By focusing the camera at different depths into the cavity of the BB, it was determined that the intensity at the entrance to the conical cavity, which is at a depth of 3.94 mm inside the BB, was 1.15× that at the plane where the camera was focused during calibration. In addition, the measured intensities have to be scaled up 1.1×, to account for the reflection of 8.9% of the blackbody radiation by the rake face of the YAG tool during the calibration process. This loss is not sustained by IR radiation emitted by the chip surfaces in intimate contact with the tool, directly into the tool.

It was found that the intensity per unit exposure time, counts/ms, was nearly the same for each temperature, regardless of whether the blackbody was heating up or cooling down, and independent of exposure time. The power law curve

$$T = 1036.7\left(\frac{S}{\varepsilon t}\right)^{0.065} \qquad (1)$$

where S is the signal (background subtracted intensity), ε is the emissivity of the surface into YAG, and t is the exposure time in milliseconds, provided a good fit to the temperature as a function of the measured average counts/ms (S/t), with an rms error of 1.09 K. The fit exponent of 0.0645 compares well with the exponent of 0.0655 calculated using Planck's law, the quantum efficiency of the optics provided by the camera manufacturer [23], and the spectral response provided by the microscope manufacturer for a typical objective.

DATA PROCESSING

From each cutting experiment, the image recorded over the second full revolution of steady cutting is processed, if it is observed to be clean, without any visible macro-chipping of the tool edge, as shown in **Figure 3**. The background image is subtracted and the counts S at each pixel is converted into temperature using Equation 1 using the known exposure time t.

A careful survey of the results available in the literature for the emissivity of polished Ti-6Al-4V in the high temperature regime of interest to us (from 900 K to 1400 K) was carried out, and it was found that the emissivity of polished Ti-6Al-4V into air is likely to be between 0.45 (that of pure titanium) and 0.55 (the higher end of the range for polished Ti-6Al-4V) in the effective wavelength range of interest here [25,26]. The mean of the estimated range, 0.5, is taken here to be the emissivity of the chip.

The index of the medium surrounding a surface changes its emissivity. Using literature values for the refractive indices and extinction coefficients of titanium and YAG in equation 3.13 in Howell et al. [27], the emissivities into air and into YAG are found to be 0.45 and 0.63, respectively; i.e., the emissivity into YAG is 1.41× that into air. Due to the fact that the Ti-6Al-4V chip is emitting radiation directly into YAG, the estimated emissivity of the chip into air (0.5) has to be increased to 0.71 (by the factor of 1.41) for use in Equation 1 in the data processing.

Using the measurement equation above, a detailed study of the uncertainty in temperature has been carried out as a function of source temperature. The very small exponent in equation 1 causes the relative uncertainty in temperature due to uncertainties in signal and emissivity to be only one-fifteenth that of the relative uncertainty in these inputs. The

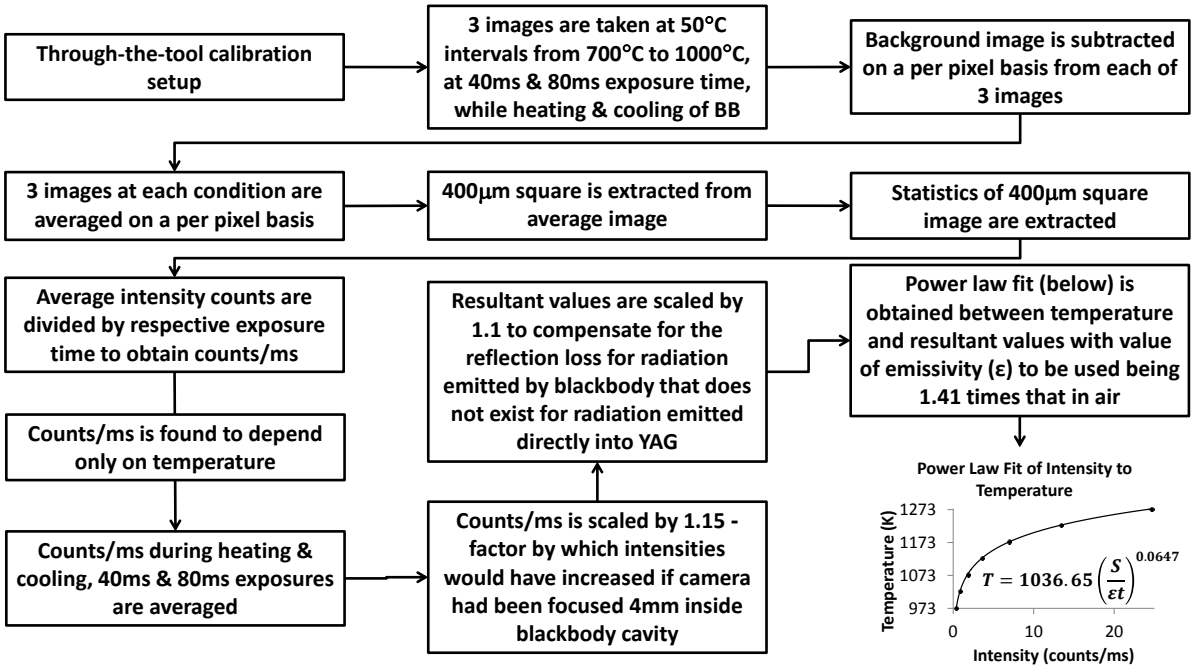

Figure 4 Flowchart showing the steps in the calibration process.

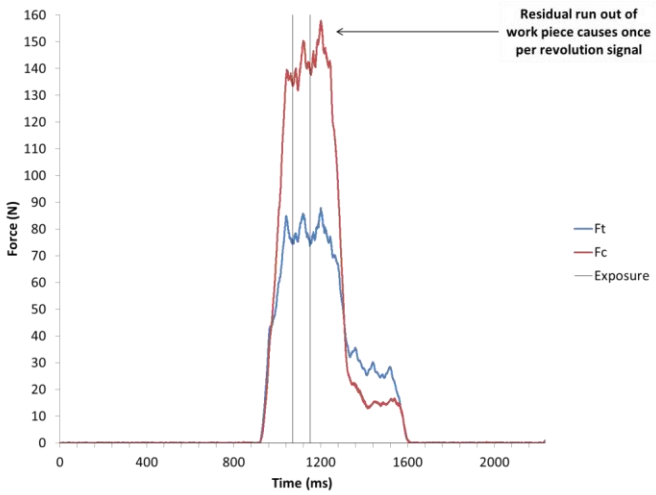

Figure 5 Example thrust and cutting forces obtained from a cut at 1 m/s speed and 50 µm feed. The beginning and end times of the exposure of the camera are also shown.

components due to emissivity uncertainty (estimated using the range of emissivity values found in the literature) and due to blackbody temperature uncertainty are nearly constant, between 2 K and 3 K. The combined uncertainty is dominated by the camera noise at lower temperatures, which limits the lower limit of measurable temperatures. The combined uncertainty was found to be less than 9 K for all signal values greater than 25 counts, and to keep the uncertainty of all reported values less than 10 K, intensity values less than 25 counts were set equal to 25 counts. On account of this, the lower bound of temperatures that can be resolved in the full-field temperature maps reported here corresponds to 983 K for t = 80 ms, and to 1030 K for t = 40 ms.

RESULTS

A typical set of forces is shown in **Figure 5**, showing small peaks likely due to non-concentricity of the outer and inner diameters of the tube, that causes the wall thickness of the tube to cycle once per revolution. The time between each of the peaks corresponds to one revolution of the tube, which is 80 ms for a cutting speed of 1 m/s and 40 ms for 2 m/s. The cutting and thrust forces ramp up to steady state over the first revolution. Following this there are two more turns at constant feed, that result in nearly constant thrust force, but a slightly increasing cutting force. The forces decrease linearly during the last revolution when the feed is zero, and then remain at a constant small value for two more revolutions before the tube is withdrawn out of contact, on account of the backlash in the ball-screw of the feed slide. The average cutting force is about 145 N and the average thrust force is about 80 N for the cutting condition shown, which are comparable to those obtained with carbide tools.

The first cutting experiment with a new tool typically shows clean images without visible chipping of the tool, as in **Figure 3**. Thereafter, the cutting edge is found to slowly degrade by chipping. All results reported here are from the first cut with a clean cutting edge.

Figure 6 shows temperature maps obtained for two cuts at cutting speeds of 1 m/s and 2 m/s. The mirror symmetry of the temperature map about the cutting edge is used to locate the cutting edge, as shown annotated here and in **Figure 3** The chip material is in contact with the rake face until it leaves contact and curls away from the rake face. In **Figure 6**(b), interference fringes are visible once the chip has left contact with the rake face. In the region of contact, the tool temperature can be expected to be very close to that of the chip due to the intimate contact between the chip and the tool due to the high contact pressure, which causes the contact thermal resistance to be negligible. Note that the fringe ranges in the images are different, and the peak temperature at 2 m/s is about 140 K greater than that at 1 m/s, while the pattern of the distribution is the same.

One-dimensional temperature profiles along the middle of the chip, showing the variation of temperature with increasing distance from the cutting edge, are obtained by averaging the temperature map along the cutting edge, in the region in the middle that is free of end effects. In the profiles shown in **Figure 7**, the temperature increases with increasing distance from the cutting edge in the chip flow direction, reaches a maximum, and then begins decreasing. **Figure 7** also shows a comparison of the temperature profiles for two cutting speeds, from which it can be noted that the peak temperature changes from 1179 K (906 °C) at 1 m/s to 1310 K (1037 °C) at 2 m/s. It is very interesting to note that due to the higher cutting speed, the temperature at the cutting edge is itself higher, and the gradient in temperature is nearly the same. The increase in temperature from that at the cutting edge to the peak value is of the order of 100 K to 130 K for the cutting experiments reported here. To the right of the peak temperature, over the second half of the contact length, the temperature of the interface starts decreasing even though the chip is still in contact with the tool and the sliding action is producing frictional heat. **Figure 7** also shows the expanded uncertainty (k = 2) in the temperatures computed for each point by propagation of the uncertainties in the various terms of Equation 1. For all points, the expanded uncertainty is within 6 K.

DISCUSSION

Full-field thermographs of the time averaged steady state temperature at the chip-tool interface have been acquired with a remarkably low expanded uncertainty in the measured temperature, less than 18 K for the temperatures reported here, and better than 10 K for temperatures above 1049 K (776 °C).

The most important feature of the results is that very

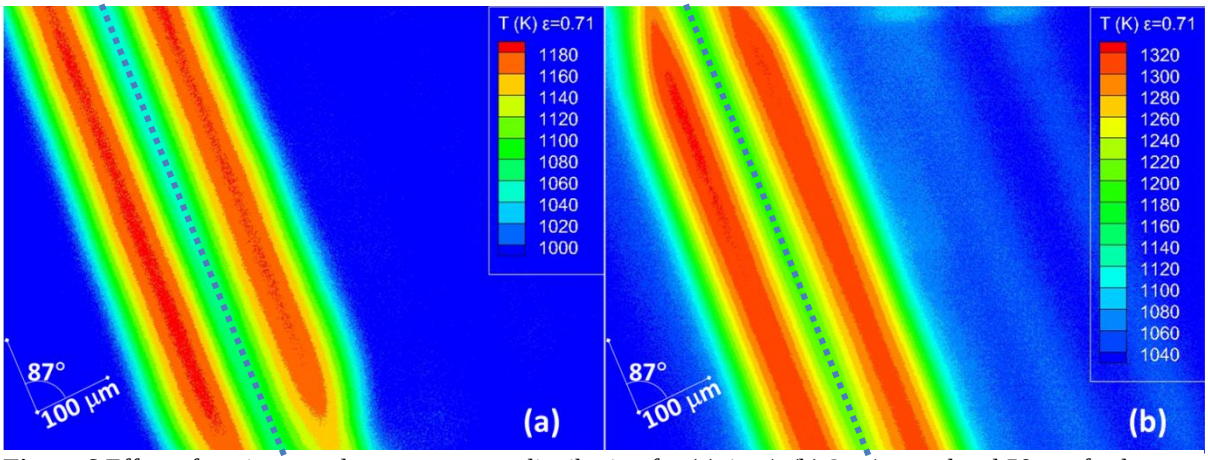

Figure 6 Effect of cutting speed on temperature distribution for (a) 1 m/s (b) 2 m/s speed and 50 µm feed. The dotted line shows the cutting edge. Note that the fringe ranges are different and that the peak temperature is about 140 K higher.

high temperatures of the order of 1273 K (1000 °C) are encountered along the rake face of the cutting tool. Even at the cutting edge, the temperature is fairly high, ranging from 1050 K to 1200 K. For titanium, these high temperatures can be rationalized based on the high strength, low thermal capacity, and low thermal diffusivity of Ti-6Al-4V.

The temperature increases rapidly from the cutting edge over approximately the first half of the contact length, by about 130 K over a distance of 75 µm. It then decreases at a higher rate over the second half of the contact length, decreasing by 200 K over a distance of 100 µm. Thereafter, the rate of decrease of temperature abruptly reduces, and the temperature decreases only about 50 K over 350 µm. The location where the chip leaves contact with the tool can be estimated by identifying the point beyond which the chip starts cooling at a fairly constant rate. From this, it can be clearly noted that the peak temperature is reached at about one-half the length of contact.

During the calibration process, one potential reason why temperatures may have been overestimated in the work by Muller-Hummel and Lahres [20] became clear. The emissivity of metals when in intimate contact with a tool made of high refractive index material is significantly higher than the emissivity into air. The higher the refractive index of the tool material (as is the case with the thick chemical vapor deposition (CVD) diamond window used by them), the more significant this effect would be.

The images shown here comprise a record of the "steady state" time averaged intensity of radiation emitted by the chip material along the rake face. The images don't show any sharp features because they are blurred by the motion of the chip, and are the record of the time averaged intensity emitted by the chip from different spatial locations.

For the purpose of validating finite element analyses, the fact that the tool material chosen is not used in commercial applications is not important. So long as the thermal properties of the tool material are accurately known, temperature measurements made through these transparent tools can be used to refine the material model for the work piece and the friction model used for the interface, until the predicted values coincide with the measured values. While the friction model to be used for other tool materials and coatings will be different, the material model developed for the workpiece can be used with confidence for all other simulations involving this work material.

CONCLUSIONS

It is demonstrated that hard to machine alloys such as Ti-6Al-4V in the hard (solution-treated and annealed, STA) temper can be successfully machined using transparent cutting tools made of YAG. The present study is the first successful effort in which Ti-6Al-4V has been cut with transparent tools and the distribution of temperature at the chip-tool interface has been measured. The temperature

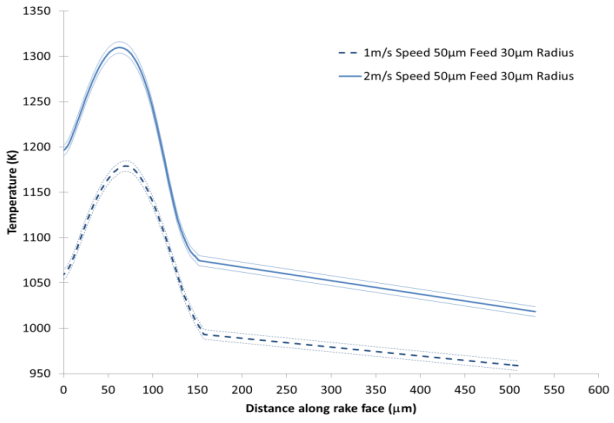

Figure 7 Effect of cutting speed on temperature profile. The expanded total uncertainty shown around the profiles is less than 6 K at all points.

increases from the cutting edge to the mid-point of the contact length, and then decreases until the end of contact. Peak temperatures of 1179 K and 1310 K (1037 °C) have been found for cutting at 1 m/s and 2 m/s cutting speeds, respectively, and 50 µm/rev feed. The accuracy and the spatial resolution of the data presented here permits researchers to use this data to verify and fine-tune material and friction models used in simulations of cutting.

ACKNOWLEDGEMENTS

Support provided by the National Science Foundation through grant number (1000819, Program Managers George Hazelrigg and Zhijian Pei) is gratefully acknowledged. Support provided by the National Institute of Standards and Technology, to VM via an IPA with Wichita State University, and to TM via a Measurements Science and Engineering research grant (Project Manager Alkan Donmez) is also gratefully acknowledged. This work could not have been completed without the generous two week loan of a 19708-S1 miniature cavity blackbody source by Electro-Optical Industries (Brent Lindstrom), which is hereby gratefully acknowledged. Valuable discussions with Howard Yoon of NIST and thorough reviews of the manuscript by Brandon Lane, Alkan Donmez, and Kevin Jurrens of NIST are gratefully acknowledged.

REFERENCES

[1] Trent, E.M., 1984. Metal Cutting. Butterworths, London.

[2] Madhavan, V., Chandrasekar, S., & Farris, T.N., 2002. Direct observations of the chip-tool interface in the low speed cutting of pure metals. Journal of Tribology, 124/3, 617-626.

[3] Ackroyd, B., Akcan, N.S., Chhabra, P., Krishnamurty, K., Madhavan, V., Chandrasekar, S., Compton, W.D., & Farris, T.N., 2001. Exploration of contact conditions in machining. Proceedings of the Institution of Mechanical Engineers, Part B: Journal of Engineering Manufacture, 215/4, 493-507.

[4] Challen, J.M., & Oxley, P.L.B., 1983. Slip line fields for explaining the mechanics of polishing and related processes. International Journal of Mechanical Sciences, 26, 403-418.

[5] Childs, T. H. C., Maekawa, K., Obikawa, T., & Yamane, Y., 2000. Metal machining: Theory and applications, Arnold, England.

[6] Stephenson, D.A., 1993. Tool-work Thermocouple Measurements: Theory and Implementation Issues. Journal of Engineering for Industry, 115, 432-437.

[7] Usui, E., Shirakashi, T., & Kitagawa, T., 1978. Analytical prediction of three dimensional cutting process — 3. Cutting temperature and crater wear of carbide tool. Journal of Engineering for Industry, 100, 236-243.

[8] Wright, P., & Trent, P., 1974. Metallurgical appraisal of wear mechanisms and processes on high speed tools. Metals Technology, 13.

[9] Lo Casto, S., Lo Valvo, E., & Micari, F., 1989. Measurement of temperature distribution within tool in metal cutting experimental test and numerical analysis. Journal of Mechanical Working Technology, 20, 35-46.

[10] Miller, M. R., Mulholland, G., & Anderson, C., 2003. Experimental cutting tool temperature distributions. Journal of Manufacturing Science and Engineering, 125, 667-673.

[11] M'Saoubi, R., & Chandrasekaran, H., 2004. Investigation of the effects of tool micro-geometry and coating on tool temperature during orthogonal turning of quenched and tempered steel. International Journal of Machine Tools and Manufacture, 44, 213-224.

[12] Boothroyd, G., 1963. Temperatures in orthogonal metal cutting. Proceedings of Institute of Mechanical Engineering, 177, 789-802.

[13] Sutter, G., Faure, L., Molinari, A., Ranc, N., & Pina, V., 2003. An experimental technique for the measurement of temperature fields for the orthogonal cutting in high speed machining. International Journal of Machine Tools and Manufacture, 45, 671-678.

[14] Hijazi, A., Sachidanandan, S., Singh, R., & Madhavan, V., 2011. A calibrated dual-wavelength infrared thermometry approach with non-greybody compensation for machining temperature measurements. Measurement Science and Technology, 22(2), 025106-025118.

[15] Jaspers, S., Dautzenberg, J., & Taminiau, D., 1998. Temperature measurement in orthogonal metal cutting. The International Journal of Advanced Manufacturing Technology, 14, 7-12.

[16] Davies, M.A., Yoon, H., Schmitz, T.L., Burns, T.J., & Kennedy, M. D., 2003. Calibrated thermal microscopy of the tool–chip interface in machining. Machining Science and Technology, 7, 167–190.

[17] Pednekar, V., Madhavan, V. and Adibi-Sedeh, A.H., Investigation of the transition from plane strain to plane stress in orthogonal metal cutting. ASME International Mechanical Engineering Congress & Exposition, Anaheim, California, Nov. 2004.

[18] Muller-Hummel, P., & Lahres, M., 1994. Infrared temperature measurement on diamond coated tools during machining. Diamond and Related Materials, 3, 765-769.

[19] Muller-Hummel, P., & Lahres, M., 1995. Quantitative measurement of temperatures on diamond-coated tools during machining. Diamond and Related Materials, 4, 1216-1221.

[20] Muller-Hummel, P., Lahres, M., Mehlhose, J., & Lang, G., 1997. Measurement of temperature on diamond coated tools during machining films and

technology. Diamond Films and Technology, 7(4), 219-232.

[21] Narayanan, V., Krishnamurthy, K., Chandrasekar, S., Farris, T.N., & Madhavan V., 2001. Measurement of the temperature field at the chip-tool interface in machining. Symposium on Fundamental Issues in Machining, ASME IMECE 2001. Paper # MED 21310. New York.

[22] Mah, T.I., & Parthasarathy, T.A., 1997. Effects of temperature, environment, and orientation on the fracture toughness of single-crystal YAG. Journal of the American Ceramic Society, 80/10, 2730-2734.

[23] PCO-TECH, 2008. Sensicam QE product sheet 06/2008. Retrieved from http://www.pco.de/fileadmin/user_upload/db/products/datasheet/sensicam_qe_20080624.pdf .

[24] Hijazi, A., & Madhavan, V., 2008. A novel ultra-high speed camera for digital image processing applications. Measurement Science and Technology, 19(8).

[25] Touloukian, Y.S., & Purdue University, 1970. Thermophysical Properties of Matter: The TPRC Data Series; a Comprehensive Compilation of Data. Volume 7: Thermal Radiative Properties, Metallic Elements and Alloys. Ed. Y.S. Touloukian. New York.

[26] Milosevic N., & Aleksic, I., 2012. Thermophysical properties of solid phase Ti-6Al-4V alloy over a wide temperature range. International Journal of Materials Research, 103/6, 707-714.

[27] Howell, J.R., Siegel, R., & Menguc, M.P., 2011. Thermal Radiation Heat Transfer. 5th Edition, CRC Press.